Low Lewis Number Flames Near a Porous-Plug burner: Stability, Dynamics and Limits of Existence

Daniel Fernández-Galisteo, Carmen Jiménez, Vadim N. Kurdyumov
Energy Department, Centro de Investigaciones Energéticas, Medioambientales y Tecnológicas
28040, Madrid, Spain

1 Introduction

States of ordered (hexagonal) and disordered cellular structures have been reported in the literature for flames stabilized in porous-plug burners [1–4]. More recently, the dynamics of hexagonal and band-like cell structures were characterized numerically in [5] using fully resolved three-dimensional (3D) simulations of H_2-CO_2 flames stabilized in a porous-plug burner. Other studies have identified conditions under which flame oscillations arise within an intermediate range of mass flow rates [6, 7]. In this study, we perform numerical simulations in one, two and three dimensions employing a single-step Arrhenius chemistry model within the diffusive-thermal framework. Our objective is to demonstrate that the diffusive-thermal model adequately captures the previously reported hexagonal cellular formations. Specifically, our simulations show that all hexagonal solutions remain steady, consistent with the fuel-lean mixtures employed in [5], although we do not observe the band-like structures reported in that study. Additionally, we compare our results with the linear stability analysis of one-dimensional (1D) steady state solutions, when applicable. This reveals that the planar solution becomes unstable for mass flow rates exceeding a critical threshold, significantly lower than the product of the initial density, plug area, and laminar flame speed, consistent with the previous findings in the literature.

2 Formulation

Let us consider a uniform mass flux of perfectly mixed fuel and oxidizer emerging from a porous plug that is much thicker than the thermal thickness of the flame that is formed at a certain distance downstream of the plate; see Fig.1. The thermal conductivity of the plug is assumed sufficiently high to maintain the gas temperature in the plug constant and equal to the upstream temperature T_0. The mixture is assumed to be fuel-lean, so that the oxidizer mass fraction remains nearly constant and only the fuel mass fraction varies through chemical reactions. The chemical reaction is modeled as proportional to the fuel mass fraction with an irreversible Arrhenius-type temperature dependence.

For the sake of simplicity, we adopt a diffusive-thermal model, with all the thermodynamic and transport coefficients assumed to be constant. The dimensionless equations for the conservation of energy and

Correspondence to: d.galisteo@ciemat.es

chemical species read

$$\frac{\partial \theta}{\partial t} + m\frac{\partial \theta}{\partial x} = \nabla^2 \theta + \omega, \tag{1}$$

$$\frac{\partial Y}{\partial t} + m\frac{\partial Y}{\partial x} = \frac{1}{Le}\nabla^2 Y - \omega, \tag{2}$$

where $\nabla^2 = \partial^2/\partial x^2 + \partial^2/\partial y^2 + \partial^2/\partial z^2$ and the reaction rate takes the form

$$\omega = \frac{\beta^2}{2Le\, u_p^2} Y \exp\left\{\frac{\beta(\theta-1)}{1+\gamma(\theta-1)}\right\}, \tag{3}$$

where $\theta = (T - T_0)/(T_{\rm ad} - T_0)$ is the dimensionless gas temperature and $Y = Y_F/Y_{F_0}$ is the dimensionless fuel mass fraction. Space and time coordinates have been scaled by the thermal flame thickness, $\delta_T = \mathcal{D}_T/S_L$, and the flame time, $\mathcal{D}_T/S_L^2$, where $\mathcal{D}_T$ is the thermal diffusivity of the mixture and S_L the burning velocity of the planar adiabatic flame. The dimensionless parameters that appear in the above formulation are the Zel'dovich number $\beta = E(T_{\rm ad} - T_0)/\mathcal{R}T_{\rm ad}^2$, the heat release coefficient $\gamma = (T_{\rm ad} - T_0)/T_{\rm ad}$, the fuel Lewis number Le, with $T_{\rm ad} = T_0 + QY_0'/c_p$ the adiabatic flame temperature, and the reduced mass flow rate $m = U/S_L$, with U the inflow velocity. The factor $u_p = S_L/U_L$ in (3) is introduced to take into account the difference between the asymptotic ($\beta \ll 1$) value of the planar burning velocity U_L and the value of S_L for finite β. This ensures that the speed of a computed planar flame equals one for a given finite β. The value of u_p is 1.0061 for $\beta = 10$, $\gamma = 0.7$ and $Le = 0.3$.

Periodic boundary conditions are applied along the y and z-directions, together with

$$\theta = m(Y - 1) - Le^{-1}\partial Y/\partial x = 0 \tag{4}$$

at the plug surface $x = 0$. Far downstream, $x \to \infty$, we apply the weak condition

$$\partial^2\theta/\partial x^2 = \partial^2 Y/\partial x^2 = 0. \tag{5}$$

Equations (1)-(2) are integrated using a finite-difference second-order scheme with three-point approximation for space derivatives on a uniform grid with resolution $\Delta_x = \Delta_y = \Delta_z = 0.2$, which sets about 5 points in the inner reaction zone. Although the grid resolution seems coarse, it suffices to show first preliminary results for the present piece of work.

3 Results

The steady, one-dimensional version of Eqs. (1)-(2) with boundary conditions (4)-(5) are first solved. In particular, the obtained standoff distance, x_f (the distance from the flame, where the reaction rate peaks, to the porous plug exit), is shown in Fig. 2 (left) as a function of the flow rate m. It is important to note that solutions for $m > 1$ are blown off and, therefore, cannot not exist in the planar form near the porous-plug burner.

A subsequent linear stability analysis of these steady planar flame solutions is conducted to generate Fig. 2 (right). For simplicity, the formulation of the stability problem is not included here but can be found in [6]. In Fig. 2 (right) the variation of the real part of the instability growth rate, λ_R, with the wave number of the perturbation, k, is shown for two different values of the mass flow. Within the range of mass flow rates investigated, the imaginary part of the growth rate remains zero. Fig. 2 (right) further indicates that cellular structures can emerge for $m \gtrsim 0.4$, while the flame remains planar for $m \lesssim 0.4$. It is interesting to note that in [5] cellular instabilities were detected for $m \gtrsim 0.7$.

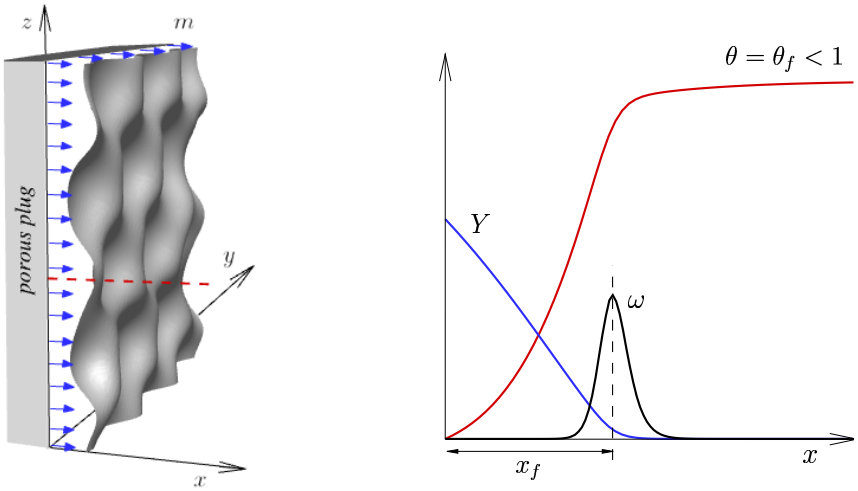

Figure 1: Left: sketch of the 3D problem showing a cellular flame structure. Right: one-dimensional distribution of temperature θ, fuel mass fraction Y and reaction rate ω along the x-direction marked with dashed line on the left figure. The definition of the standoff distance x_f is shown in the right figure.

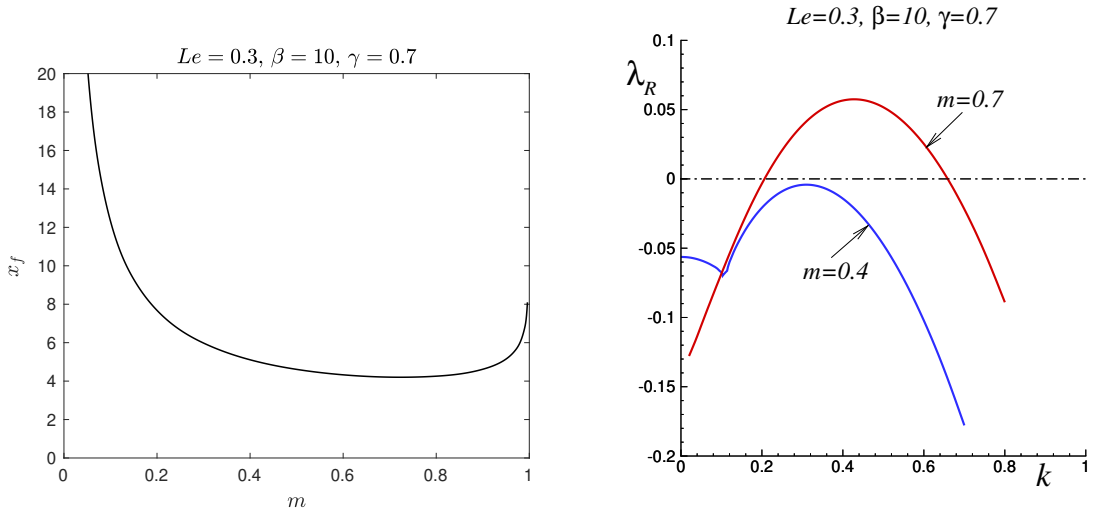

Figure 2: Left: the variation with the mass flow m of the standoff distance x_f for the one-dimensional version Right: the growth rate λ_R as a function of the wave number of the perturbation k for $m = 0.4$ and $m = 0.7$. Calculated for $\beta = 10$, $\gamma = 0.7$ and $Le = 0.3$.

The prediction of the linear stability analysis are first validated using time-dependent 2D simulations and subsequently through 3D simulations. Figure 3 shows isocontours of temperature for three different mass flows in the 2D cases. For $m = 0.5$ and $m = 0.7$, the flame exhibits cellular structures, where as for $m = 0.3$, the flame retains its planar form, consistent with the dispersion relation shown in Fig. 2 (right). The size of the cells roughly corresponds to maximum wave number inferred from Fig. 2 (right), i.e. $k \approx 0.315$.

A 3D simulation for $m = 0.7$ is presented in Fig. 4. The figure depicts the isosurface of temperature at $\theta = 0.8$, colored according to the reaction rate ω. Flame cells are observed to form a quasi-hexagonal. At this low mass flow rate, the fully resolved simulations presented in [5] report band-like structures,

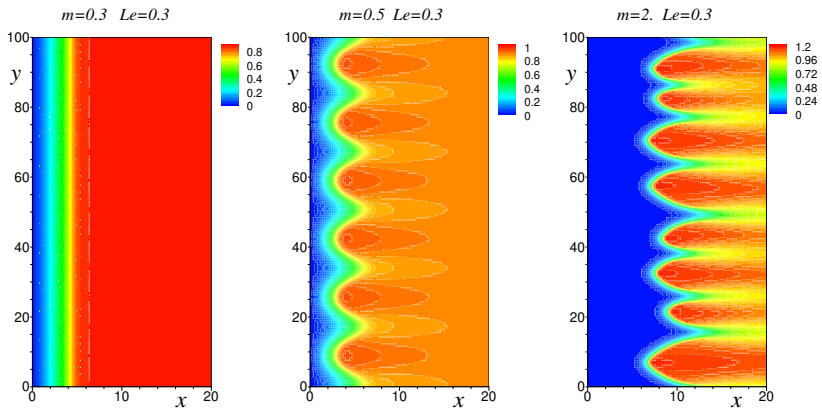

Figure 3: Examples of 2D flame solutions at different mass flows, showing the emergence of cellular flames as m is increased. Calculated for $\beta = 10$, $\gamma = 0.7$ and $Le = 0.3$.

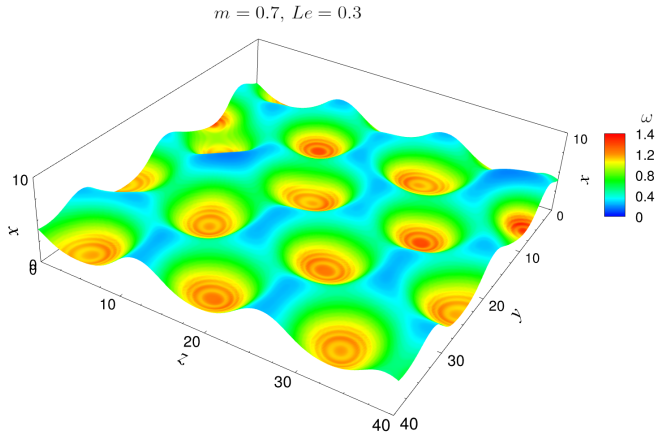

Figure 4: Isosurface of temperature at $\theta = 0.8$ colored by the reaction rate ω for a 3D flame solution at mass flow $m = 0.7$. Calculated for $\beta = 10$, $\gamma = 0.7$ and $Le = 0.3$.

which are not observed here. When the mass flow is increased to $m = 2$, as shown in Fig. 5, the number of cells increases while preserving the ordered quasi-hexagonal structure. At this high mass flow rate, the simulations presented in [5] report similar quasi-hexagonal structures. For larger lateral domains, such as 80×80 (not shown), compared to those shown in Figs. 4 and 5, i.e. 40×40, we observe emergence of disordered cell structures.

4 Conclusions

Consistent and systematic 1D, 2D, and 3D numerical simulations of flames stabilized near a porous-plug burner were performed within the framework of the diffusive-thermal model for a low Lewis number, $Le = 0.3$. Preliminary 2D and 3D numerical simulations (obtained using a coarse grid resolution) revealed cellular structures (in hexagonal arrangements in the 3D cases) above a critical mass flow rate value, in agreement with the corresponding hexagonal cellular structures reported previously [1–5], although the band-like structures reported in [5] are not found here. Finally, the number of cells that can be accommodated in the domain depends on the mass flow, while the ordered or disordered nature of the state seems to depend on the size of the lateral computational domain employed in the simulations.

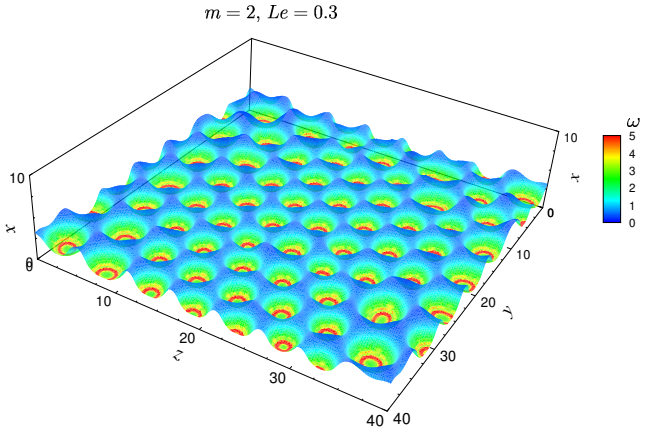

Figure 5: Isosurface of temperature at $\theta = 0.8$ colored by the reaction rate ω for a 3D flame solution at mass flow $m = 2$. Calculated for $\beta = 10$, $\gamma = 0.7$ and $Le = 0.3$.

References

[1] Markstein GH. (1951). Experimental and theoretical studies of flame front stability. J. Aeronaut. Sci. 18, 199-209.

[2] Shtilman H, Sivashinsky GI. (1990). On the hexagonal structure of cellular flames. Can. J. of Phys. 68, 768-771.

[3] Gorman M, El-Hamdi M, Robbins K. (1994). Experimental observation of ordered states of cellular flames. Combust. Sci. and Tech. 98, 37-45.

[4] Kadowaki S. (2002). Formation of cellular flames and increase in flame velocity generated by intrinsic instability. Trans. Japan Soc. Aero. Space Sci. 45, 45-52.

[5] Zirwes T, Eckart S. Zhang F, Kaiser TL, Oberleithner K, Stein OT, Bockhorn H, Kronenburg A. (2024). Structure and dynamics of hexagonal cells in H_2-CO_2 flames. Proc. Combust. Inst. 40, 105332.

[6] Kurdyumov VN, Matalon M. (2008). The porous-plug burner: Flame stabilization, onset of oscillation, and restabilization. Combust. Flame 153, 105-118.

[7] Kurdyumov VN, Sánchez-Sanz M. (2013). Influence of radiation losses on the stability of premixed flames on a porous-plug burner. Proc. Combust. Inst. 34, 989-996.